Shake-The-Box 3D particle tracking for two-pulse recordings

M. Novara, D. Schanz, A. Schröder
German Aerospace Center (DLR), Inst. of Aerodynamics and Flow Technology, Göttingen, Germany
*matteo.novara@dlr.de

Keywords: Lagrangian Particle Tracking, STB, two-pulse, IPR

ABSTRACT

The Shake-The-Box (STB, Schanz et al. 2016) three-dimensional Lagrangian Particle Tracking (LPT) technique introduced the concept of particle prediction in order to integrate the temporal domain into the particle reconstruction process based on Iterative Particle Reconstruction (IPR, Wieneke 2013). Taking advantage of long time-resolved (TR) recording sequences, the STB technique is able to cope with high particle image densities while delivering the accurate measurement of the particles position, velocity and acceleration along individual tracks. The Multi-Pulse STB (MP-STB, Novara et al. 2016a, 2019) extended the range of applicability of the algorithm to high flow velocities, where time-resolved recordings cannot be attained due to the limitation frequency of the high-speed acquisition systems, by adopting multi-pulse systems (i.e. dual illumination and imaging setup).

Nevertheless, dual-frame 3D acquisition systems, consisting in a dual-cavity laser and double-frame cameras, remain commonly used for many particle-image-based investigations in a wide range of flow velocities and applications. As a consequence, a 3D LPT approach capable of dealing with two-pulse recordings is of high interest for both the scientific community and industry.

In the present study, a Two-Pulse Shake-The-Box approach (TP-STB) is proposed, based on the advanced IPR algorithm presented by Jahn et al. 2021, in combination with the iterative scheme of reconstruction and tracking introduced for the Multi-Pulse STB algorithm development.

The performances of TP-STB are assessed by means of comparison with the results from the time-resolved STB algorithm (TR-STB) on synthetic data. Application to a nexperimental dataset of Rayleigh-Bénard-Convection proves the concept in real-life conditions.

1. Introduction

The problem of reconstructing the three-dimensional position of particle flow tracers from their projection on multiple cameras lies at the heart of several 3D particle-image-based velocimetry and Lagrangian particle tracking (LPT) measurement techniques.

While cross-correlation-based techniques such as tomographic-PIV (Tomo-PIV, Elsinga et al. 2006) make use of algebraic methods (e.g. MART, Herman and Lent 1976) to reconstruct particles as intensity peaks in a discretized voxel space, triangulation-based methods (3D-PTV, Nishino et al. 1989, Maas et al. 1993 and Iterative Particle Reconstruction, IPR, Wieneke 2013, Jahn et al. 2021) leverage epipolar geometry to reconstruct individual particles as positions and peak-intensity values in the 3D domain.

Despite the inherent differences concerning accuracy, robustness and computational cost between the two approaches, in both cases the 3D reconstruction represents a bottleneck when the spatial resolution (i.e. particle image density, indicated in particles per pixel, ppp) of the measurement is considered.

In fact, as the number of particles to be reconstructed increases (assuming constant properties of the imaging system), the reconstruction process become increasingly difficult due to the underdetermined nature of the problem. This typically results in a lower number and positional accuracy of the reconstructed particles, as well as an increasing number of spurious particles (*ghost particles*, Elsinga et al. 2011) which affect the accuracy of the measurement.

As a consequence, during the last decade, several methods have been developed to increase the performances of the reconstruction technique; an overview of these developments can be found in Scarano 2012 and Jahn et al. 2021. Among these methods, a number of techniques have been proposed to improve the accuracy of the reconstruction of instantaneous recordings by exploiting the coherence of the particle tracers moving with the flow over two or more realizations in the recording sequence.

Concerning cross-correlation-based methods, the Motion Tracking Enhancement technique (MTE, Novara et al. 2010) proposed the combined use of two or more recordings (for double-frame and time-resolved acquisition respectively) to produce an enhanced initial guess for the Tomo-PIV algebraic reconstruction algorithm; for time-resolved recording sequences, a time-marching approach was introduced by Lynch and Scarano 2015 (sequential MTE, SMTE).

On the other hand, when Lagrangian Particle Tracking techniques are considered, the Shake-The-Box algorithm (STB, Schanz et al. 2013, 2016) introduced a predictor/corrector scheme to integrate the temporal domain into the IPR-based reconstruction process. Taking advantage of long time-resolved recording sequences, where particle tracers can be followed over hundreds of realizations, the STB technique further extends the performances of IPR in terms of particle image density that can be dealt with. While Wieneke 2013 reported 0.05 *ppp* as an upper limit for IPR (already one order of magnitude larger than that typically employed for 3D-PTV single-pass triangulation), STB can deliver practically *ghost-free* tracks exceeding 0.1 *ppp* (Huhn et al. 2017, Bosbach et al. 2019); particle image densities up to 0.2 *ppp* have been successfully tackled for synthetic data (Sciacchitano et al. 2021). The combination of accurate LPT results from STB and data assimilation algorithms (FlowFit, Gesemann et al. 2016, VIC+, Schneiders and Scarano 2016) allows to further enhance the spatial resolution of the measurement and provides access to the spatial gradients (i.e. flow structures) and to the instantaneous 3D pressure field.

When high-speed flows are considered, due to the frequency limitation of current acquisition systems, time-resolved sequences of recordings are not available. In order to overcome this limitation and extend the advantages of STB to higher flow velocities, the use of multi-pulse systems (i.e. dual illumination and imaging setup) in combination with an iterative STB approach (Multi-Pulse Shake-The-Box, MP-STB) was proposed by Novara et al. 2016a; an iterative strategy based on the sequential application of IPR and particle tracking is employed to progressively reduce the complexity of the reconstruction problem. The use of multi-exposed frames (Novara et al. 2019) allows to acquire multi-pulse recordings for MP-STB making use of only a single imaging system.

While performing LPT with STB requires either the availability of time-resolved recordings (TR-STB) or the use of a relatively complex multi-pulse setup for MP-STB, dual-frame 3D acquisition systems, consisting in a dual-cavity laser and double-frame cameras, are commonly used for many particle-image-based investigations in a wide range of flow velocities and applications. As a consequence, a STB approach for two-pulse recordings is of high interest for the scientific community as it would allow to extend the benefits of accurate LPT analysis to a wider range of applications and users, as well as to enable the processing of datasets recorded with dual-frame systems (i.e. existing Tomo-PIV experiments).

These considerations motivated a number of attempts to perform Lagrangian particle tracking with dual-frame recordings.

Fuchs et al. 2016 proposed a hybrid method that leverages the robustness of tomographic PIV in order to enable carrying out 3D particle tracking for double-frame recordings. The technique makes use of tomographic reconstruction as a predictor for locating the corresponding particle images on the image plane, therefore enabling an educated triangulation procedure, followed by two-frames particle tracking.

An iterative algorithm based on IPR reconstruction, 3D cross-correlation and two-pulse tracking was used by the DLR Göttingen group to analyze the single-exposed double-frame recording relative to Case C of the 4th International PIV Challenge in 2014 (Kähler et al. 2016). The same synthetic dataset was analyzed by Jahn et al. 2017 adopting the simultaneous IPR reconstruction of the two frames combined with a particle-matching-based filtering technique; every two IPR iterations, reconstructed particles which did not form a two-pulse track (based on an approximation of the expected velocity field) were iteratively deleted to progressively reduce the complexity of the reconstruction problem.

A non-iterative 2D/3D particle tracking velocimetry algorithm was proposed by Fuchs et al. 2017. Following 3D reconstruction (Fuchs et al. 2016), a statistical analysis of all possible particle displacements within a search area is performed considering the neighbors of the particle of interest to determine the most probable displacement. The authors reported that the technique was successful in tackling images with a particle image density up to 0.06 ppp. Lasinger et al. 2020 presented a variational approach to jointly reconstruct the individual tracer particles in two time-steps, as well as the dense 3D velocity field in a hybrid Lagrangian/Eulerian model.

A novel technique for performing 3D-PTV from double-frame images (DF-TPTV) has been proposed by Cornic et al. 2020. A sparsity-based reconstruction method allows for the reconstruction of the particle tracers on a voxel grid; reconstructed particles are then tracked with the aid of a low-resolution displacement predictor from correlation, followed by a global optimizing procedure to refine the particle tracking. The DF-TPTV algorithm has been applied to experimental data from a round jet in air at 0.06 ppp.

Recently, an advanced version of the IPR algorithm has been proposed (Jahn et al. 2021), which significantly improves the performances of the reconstruction; single recordings can be

reconstructed up to a particle image density of $0.14\,ppp$ with a very low occurrence of ghost particles even at realistic conditions concerning the image noise.

In the present study, a Two-Pulse STB approach (TP-STB) is presented which makes use of the enhanced IPR algorithm combined with the iterative STB strategy commonly adopted for MP-STB (Novara et al. 2016a, 2019), and aided by velocity field prediction from Particle Space Correlation (PSC, Novara et al. 2016b). The TP-STB algorithm was successfully applied to analyze two-pulse synthetic images from the First Challenge on Lagrangian Particle Tracking and Data Assimilation (Leclaire et al. 2021) conducted in the framework of the European Union's Horizon 2020 project HOMER (Holistic Optical Metrology for Aero-Elastic Research).

Results presented in Sciacchitano et al. 2021 showed that nearly the totality of particle tracers could be reconstructed up to $0.16\,ppp$, with an almost negligible number of spurious ghost particles and a very high particle position accuracy (positional mean error magnitude of approximately $0.06\,px$).

The excellent results of the LPT and DA challenge, together with the aforementioned considerations on the relevance of dual-frame applications, motivate the present investigation.

The TP-STB algorithm is presented in section 2. A performance assessment is carried out in section 3 based on the application of TP-STB to two recordings from a time-resolved sequence, where the TR-STB results provide a reference for the *ground-truth* solution. Both synthetic data from a significantly more challenging (high image noise level) database generated within the HOMER project (Sciacchitano et al. 2022) and experimental data from a Rayleigh Bénard convection investigation (Weiss et al. 2022) have been used for the assessment (sections 3.1 and 3.2 respectively).

2. Iterative STB for two-pulse recordings

The iterative particle reconstruction/tracking strategy for TP-STB is shown in Figure 1-left; the working principle of the algorithm is based on the MP-STB processing technique from Novara et al. 2016a, 2019. The 3D particle positions and intensities are reconstructed by means of advanced IPR (Jahn et al. 2021) for both recordings in the two-pulse sequence. Then, two-pulse tracks are identified, possibly with the aid of a velocity field predictor, between the two reconstructed 3D particle fields (see section 2.1).

As the position of ghost particles mainly depends on geometrical properties (i.e. relative position of the tracers with respect to the cameras line-of-sight), the displacement of spurious peaks is typically not coherent with the flow field (Elsinga et al. 2011). For this reason, only the particles that can be tracked over the two recordings are retained; unmatched particles (in gray in Figure 1-left), possibly ghosts, are discarded (i.e. *filtering* step).

Retained particle peaks are back-projected onto the image plane (*projected images*) and subtracted from the original recordings (*recorded images*) to obtain the *residual images*; the IPR reconstruction, tracking step and evaluation of projected/residual images constitute a single STB iteration.

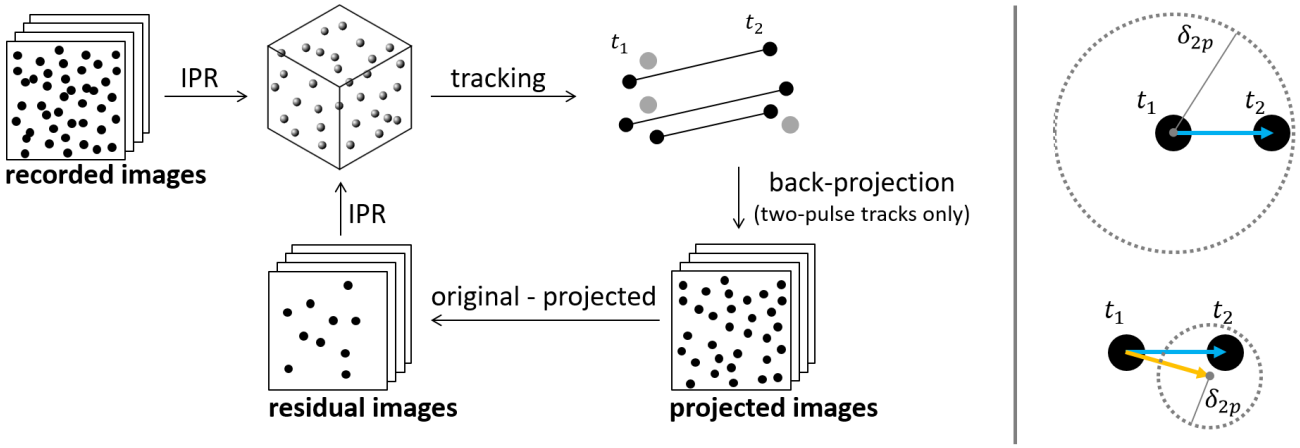

Figure 1. Left: iterative processing strategy for TP-STB (adapted from Novara et al. 2019); two-pulse tracks are indicated in black, untracked particles in gray. Right: particle tracking scheme without (top) and with (bottom) the aid of a displacement predictor (orange arrow).

Assuming that a number of tracks can be successfully identified in the first STB iteration, the residual images will exhibit a lower particle image density than the original recordings, therefore offering a progressively easier reconstruction problem for the following iterations. If a particle is erroneously discarded during the filtering step (e.g. untracked particles due to insufficiently large search radii or to an inaccurate displacement predictor field) the relative particle image will remain on the residual images, making it possible for the particle to be reconstructed and tracked at a subsequent iteration.

The number of STB iterations required to achieve convergence depends on the experimental and imaging conditions (i.e. particle image density and diameter, number of cameras, image quality); the effect of this processing parameter is discussed in the performance assessment (section 3).

2.1. Particle tracking strategy

The two-pulse particle tracking strategy is shown in Figure 1-right. A search area is established around the reconstructed particles in the first pulse (t_1); if a particle from t_2 is found within the search area, a *track candidate* is identified. If a predictor for the displacement field is available (orange arrow in Figure 1-right), the search radius δ_{2p} can be reduced to avoid ambiguities.

For each candidate, a cost function is defined as the standard deviation of the particle intensity along the track candidate (σ_I); if a velocity predictor is available, the magnitude difference between the velocity estimated from the track candidate and that from the predictor (ε_{pred}) is integrated in the cost function. The relative contribution of these two parameters to the cost function can be weighted based on the level of confidence in the particle peak intensity consistency and in the accuracy of the predictor field.

Two-pulse *tracks* are obtained by filtering the track candidates to solve possible ambiguities; among multiple candidates sharing the same particle, the one which minimizes the cost function is retained, while the others are discarded.

An additional filtering of the tracks can be applied by defining maximum accepted values for the cost function terms; tracks exhibiting values exceeding these thresholds ($\sigma_I^{max}$and ε_{pred}^{max}) are discarded from the reconstruction in order to avoid possible outliers.

For the first TP-STB iteration, an estimate of the instantaneous 3D velocity field to be used as a displacement predictor can be obtained by analyzing the two 3D point clouds reconstructed from IPR with the Particle Space Correlation algorithm (PSC, see Appendix).

The PSC consists of a 3D cross-correlation approach in the particle space; unlike for tomographic PIV, where the cross-correlation is applied to the voxel space, the PSC makes use only of the particle peak locations and intensities as obtained from IPR. An iterative procedure analogous to that proposed for the volume deformation multigrid cross-correlation technique (Scarano and Poelma 2009) can be applied to progressively increase the spatial resolution of the estimated velocity field. A tri-linear interpolation is used to evaluate the predicted displacement from the PSC result at the location of the reconstructed particles (orange arrow in Figure 1-right).

Due to the large cross-correlation volumes, the resulting velocity field from PSC (u_{PSC}) is typically strongly modulated; for subsequent STB iterations, a displacement predictor can be obtained by interpolating the scattered velocity measurements from the tracks identified in the previous iterations (u_{tracks}). Alternatively, a constant shift can be used as a displacement predictor (u_{const}); $u_{const} = 0$ corresponds to a situation where no displacement predictor is used (Figure 1-right-top).

A different set of particle tracking parameters (i.e. search radius δ_{2p}, cost function parameters $\sigma_I, \varepsilon_{pred}$, relative weights and threshold values (σ_I^{max}, ε_{pred}^{max}), the use and choice of velocity predictor ($u_{const}, u_{PSC}, u_{tracks}$)) can be employed for each TP-STB iteration, depending on the experimental conditions and image quality.

3. Performance assessment: comparison with time-resolved STB

Typically, the performances of a novel algorithm are assessed by applying it to a dataset where the *ground-truth* solution is known (i.e. synthetically generated dataset).

On the other hand, the results presented in Sciacchitano et al. 2021 concerning the assessment of STB applied to time-resolved recordings, show that TR-STB is capable to provide a close-to-perfect reconstruction up to 0.2 ppp with a very low number of ghost particles ($< 0.1\%$) and a high particle peak positional accuracy (positional mean error magnitude $< 0.05\ px$).

As a consequence, it can be assumed that, under a wide range of particle image densities and imaging conditions, the results offered by TR-STB provide an accurate reference for the actual ground-truth 3D particle distribution. Therefore, in the present study, the performance assessment of TP-STB is carried out by analyzing a two-pulse recording sequence extracted from a longer acquisition, where the reference solution is obtained from a TR-STB analysis in the converged state (Schanz et al. 2016).

This approach offers the twofold advantage of allowing the assessment of the performances of TP-STB based on a synthetic dataset where the actual ground-truth is not known (HOMER internal database, Sciacchitano et al. 2022, section 3.1) and on experimental data from a time-resolved 3D investigation (Rayleigh Bénard convection, Weiss et al. 2022).

3.1. Synthetic dataset: HOMER Lagrangian Particle Tracking database

A detailed description of the HOMER LPT database can be found in Sciacchitano et al. 2022; synthetic images from a 3D imaging system have been generated based on a simulation of the air flow around a cylinder in ground effect, where the wall contains a flexible oscillating panel. Among the several cases within the database, a time-resolved sequence of recordings from a four-camera system is produced, where particle images with a significant noise level have been generated at 0.05 and 0.12 ppp. For each particle image density, a two-pulse sequence is analyzed by means of TP-STB; as mentioned above, performances in terms of reconstruction positional accuracy and velocity estimate error are assessed against a result extracted from a converged time-resolved STB (Schanz et al. 2016) analysis.

The simulated free-stream velocity V_∞ is 10 m/s, the cylinder has a diameter D of 10 mm and it is located 15 mm upstream of the upstream edge of the 100×100 mm panel at a distance of 10 mm from the undeformed wall location ($Z = 0$ mm). The X axis is aligned with the streamwise direction, the wall-normal Z axis is directed away from the wall and the spanwise Y axis orientation follows the right-hand rule.

The measurement volume spans $100 \times 100 \times 30$ mm^3 in the X, Y and Z directions respectively; the 1920×1200 px camera sensors have a pixel pitch of 10 μm. The four cameras are arranged in in-line configuration with viewing angles of $-30°, -10°, +10°$ and $+30°$ with respect to the Z axis; the average digital resolution is approximately 10.94 px/mm.

The time-resolved sequence (TR) contains 501 recordings with a time separation between pulses of 20 μs; recordings $330 - 331$ have been chosen for the TP-STB analysis.

Approximately 52,000 and 114,000 tracks are identified by the TR-STB analysis for the 0.05 and 0.12 ppp cases. The ground-truth reference result from TR-STB for recording 330 is shown in Figure 2-left for the 0.12 ppp case; tracked particles are indicated by markers color-coded by the streamwise velocity component u (details on the TR-STB analysis can be found in Sciacchitano et al. 2022).

A detail of the original particle images for camera 2 is presented in Figure 2--right for both particle image densities; due to the high image noise level, before TP-STB processing, a constant value of 130 $counts$ is subtracted from the recorded images.

The main processing parameters are summarized in Table 1. The TP-STB analysis was carried out applying 11 STB iterations. The IPR settings have been optimized for the 0.12 ppp case and applied

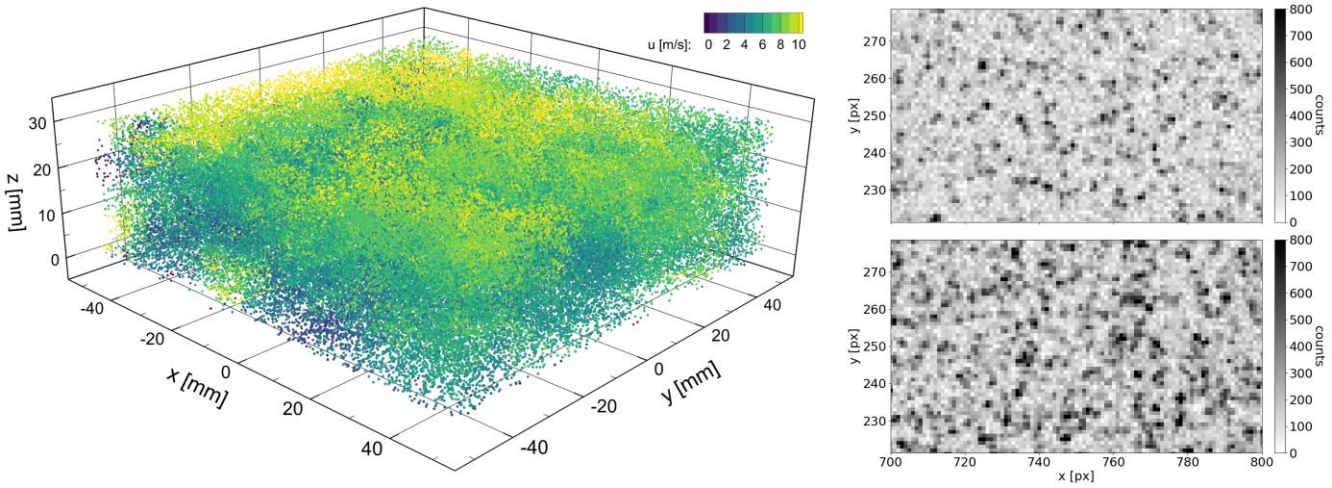

Figure 2. Left: ground-truth reference result from TR-STB for 0.12 *ppp*; approximately 114,000 particles color-coded by streamwise velocity component. Right: details of particle images at 0.05 (top) and 0.12 *ppp* (bottom).

for the lower seeding density as well for sake of consistency and ease of description; however, for the 0.05 *ppp* case a leaner processing could have sufficed to produce results of the same quality. A single 3D particle field is reconstructed in about 2 and 1 minutes for 0.05 and 0.12 *ppp* respectively; as the particle image density on the residual images decreases with the STB iterations so does the IPR processing time, depending on the fraction of tracks successfully reconstructed in the previous iterations. For a detailed description of the IPR algorithm and settings used within the TP-STB the authors refer to Jahn et al. 2021.

The displacement field predictor was estimated by PSC with a final cross-correlation volume of $20 \times 20 \times 5\ px$ (approximately $1.8 \times 1.8 \times 0.45\ mm^3$). The search for two-pulse track candidates was conducted without the aid of a predictor field (*search* predictor in Table 1 set to $u_{const} = 0$); instead, a large enough search radius (4 px) was used which ensures that even the largest particles displacements with the time separation between the pulses (estimated as $\approx 2.5\ px$) can be captured. On the other hand, the displacement predictor fields u_{PSC} and u_{tracks} have been used to

STB iteration(s)	**1**	**2 - 11**
Main IPR parameters		
Number of outer iterations	50	
2D peak intensity threshold [counts]	100	
Allowed triangulation error [px]	$0.4 - 1.0$	
Number of shaking iterations	8	
Particle tracking parameters		
Predictor (*search*/*residual*)	$u_{const} = 0$ / u_{PSC}	$u_{const} = 0$ / u_{tracks}
Search radius δ_{2p} [px]	4.0	
Cost function terms (weight factor)	σ_I (0.5) / ε_{pred} (1.0)	
σ_I^{max} [counts] / ε_{pred}^{max} [m/s]	∞ / 1.0	∞ / $1.0 - 10.0$

Table 1. Summary of TP-STB processing parameters for the synthetic test case.

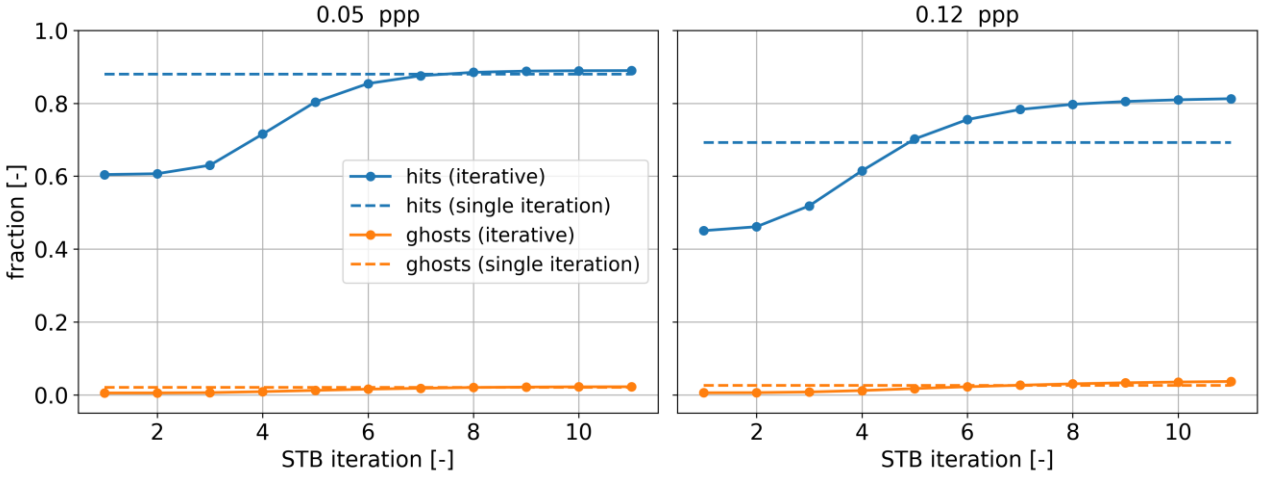

Figure 3. Fraction of reconstructed tracks from TP-STB with respect to the number of tracks from the reference TR-STB solution for both particle image densities. The fraction of correctly reconstructed tracks (*hits* in blue) and of ghost tracks (*ghosts* in orange) are shown for a single iteration (dotted line) and for the complete iterative TP-STB strategy.

evaluate the cost function term ε_{pred} (*residual* predictor in Table 1); a linearly increasing value of ε_{pred}^{max} is used to filter out possible outliers.

The performance assessment of the TP-STB results follows the same approach presented in Sciacchitano et al. 2021, 2022; a reconstructed particle is considered correct (i.e. *hit*) if a reference particle (from TR-STB) is found within a radius of 1 px. On the other hand, a particle is considered a *ghost* either when no reference particle is present in its vicinity, or when a found reference particle has already been matched to a closer reconstructed particle (i.e. when two particles are reconstructed near a reference particle, the closest one is labelled as *hit* and the other one as *ghost*). As only particles that could be tracked between the two pulses are considered for the analysis, the terms *particle* and *track* are used interchangeably in the present document.

The fraction of correct and ghost particles as obtained from the TP-STB analysis of both particle image density levels is presented in Figure 3 as a function of the number of STB iterations applied. The dotted lines refer to the result of a TP-STB processing where only one STB iteration was applied; this situation reflects the performances of two-pulse particle tracking applied to the individual IPR reconstruction of the two recordings.

The same tracking scheme has been applied for both the iterative and the single-iteration TP-STB. For the single-iteration case, the iterative tracking parameters presented in Table 1 are applied to the same 3D point clouds from IPR, and only the final result is shown in Figure 3. On the other hand, the rather conservative tracking parameters used for the first iterations (i.e. ε_{pred}^{max}) are responsible for the lower number of reconstructed tracks attained by the iterative method for STB iterations $1-5$.

Due to the already excellent performances of the single-recording enhanced IPR (Jahn et al. 2021), the beneficial effect of the iterative STB scheme depicted in Figure 1-left can only be appreciated in

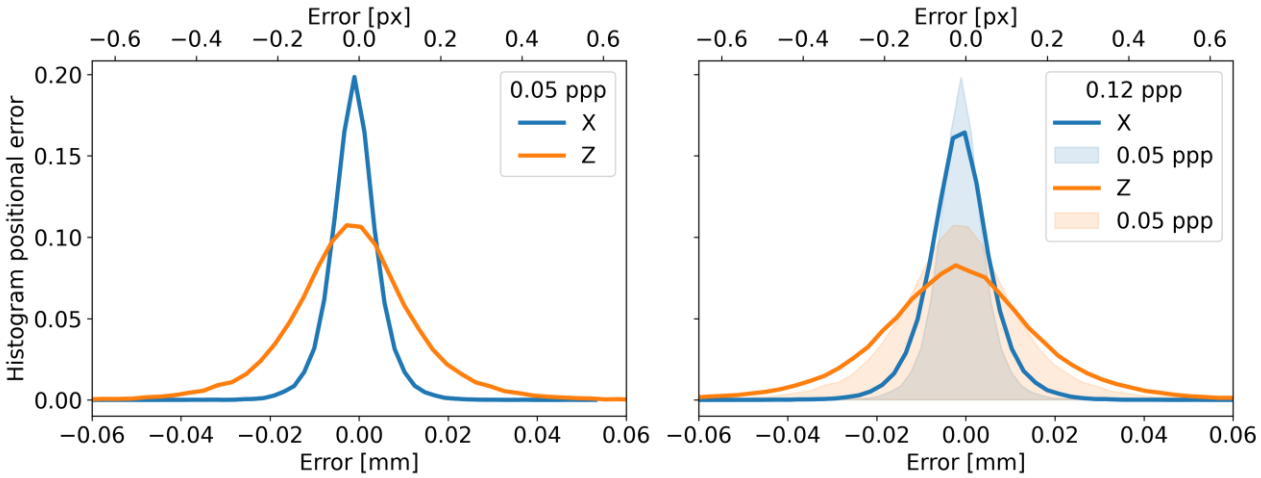

Figure 4. Histograms of the particle peak positional error for the streamwise (X in blue) and wall-normal (Z in orange) components for 0.05 and 0.12 ppp. Right: results from the 0.05 ppp case shown as shaded areas for sake of comparison.

the higher seeding density conditions; for 0.12 ppp, 12% more tracks can be correctly identified when an iterative approach is adopted ($\approx$ 81%) with respect to the single iteration result ($\approx$ 69%). On the other hand, the ghost particle level remains low in both cases ($\approx 2-3\%$). When the fraction of spurious particles is considered, it is interesting to note that the ghost level for a single-recording IPR reconstruction (i.e. no particle is discarded when failing to build a two-pulse track) is approximately 7% and 16% for 0.05 and 0.12 ppp respectively. This result shows once again the significant impact of exploiting the time information embedded in a sequence of recordings.

Given the better performances in terms of tracks yield, the results presented in the remainder of this section refer to the iterative TP-STB processing results; the fraction of correctly reconstructed tracks in the converged state is approximately 89% (46,700 tracks) and 81% (93,600 tracks) for 0.05 and 0.12 ppp respectively.

The analysis of the 3D particle peak positional accuracy is carried out by comparing the TP-STB results with the reference TR-STB solution making use of the matched particles (*hits*) for both seeding densities; the histograms of the errors in the streamwise (X) and wall-normal (Z) directions are presented in Figure 4. The results in the spanwise component (Y) are not shown as they resemble closely those for the X direction. For the low seeding density case (Figure 4-left), the root-mean-square (RMS) errors for the X and Z positions are approximately 5.6 μm (0.06 px) and 14.6 μm (0.16 px) respectively; the 2.6 factor between the accuracy in the two directions can be ascribed to the viewing direction of the imaging system being aligned with the wall-normal direction (Z). For the 0.12 ppp case, due to the higher complexity of the reconstruction problem (i.e. overlapping particle images), as expected, the positional errors increase to 7.6 μm (0.08 px) and 19 μm (0.21 px) for X and Z respectively. The results shown in Figure 4 compare well with those presented in Sciacchitano et al. 2022, confirming that the TR-STB method is capable of providing a good approximation of the actual ground-truth particle distribution.

Please note that the relatively high positional errors are mainly attributed to the high noise levels and the broad particle size distribution, which inhibits the detection of over 20% of the particles even for TR-STB (see Sciacchitano et al. 2022); when dealing with lower image noise levels, significantly higher accuracies can be achieved (see Sciacchitano et al. 2021).

3.2. Experimental dataset: Rayleigh Bénard convection flow

The performance assessment of TP-STB based on experimental data is carried out by analyzing a two-pulse sequence from the time-resolved recordings from the Rayleigh Bénard convection cell investigation presented by Weiss et al. 2022.

As for the analysis presented in the previous section, the results from TR-STB are taken as a reference of the unknown ground-truth 3D particle tracks field.

The convection flow is issued within a rectangular cell of $320 \times 320 \times 20\ mm^3$ filled with water; a heated copper plate is located at the bottom of the cell, while a cooled borosilicate glass plate is used at the top in order to provide optical access for the imaging system (Figure 5-left).

The applied temperature difference between the top and the bottom plate varies between 2 and 20 K. The flow was seeded with fluorescent 50 μm polyethylene microspheres, illuminated by two pulsed UV-LED arrays. A detailed description of the experimental setup can be found in Weiss et al. 2022.

A system of six scientific CMOS cameras was operated at a frequency $f_{acq} = 10 - 40\ Hz$ to acquire time-resolved sequences of recordings; a detail of a $2160 \times 2560\ px$ camera image is shown in Figure 5-right.

The particle image density is approximately $0.075\ ppp$; around 332,000 instantaneous particles are successfully reconstructed and tracked by the TR-STB algorithm.

In order to increase the dynamic range of the measurement, a time separation of three frames has been chosen between the two recordings used for the two-pulse reconstruction; given a digital resolution of approximately $7.15\ px/mm$, a maximum particle displacement of 11 px is expected for the case presented in this section ($f_{acq} = 19\ Hz$, maximum flow velocity magnitude of $V_{max} \approx 0.01\ m/s$).

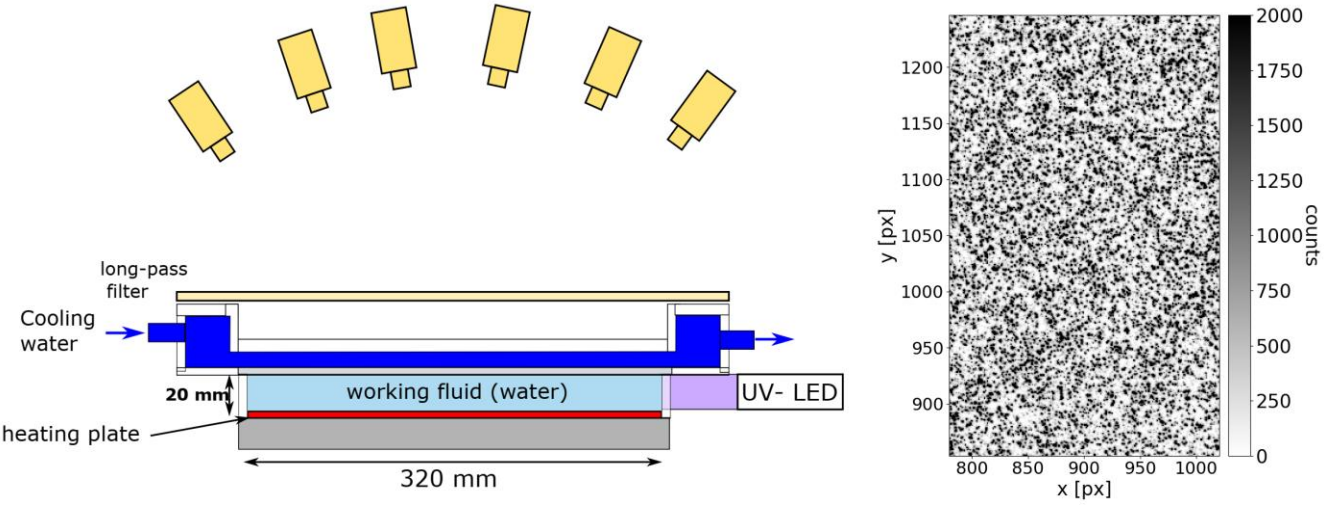

Figure 5. Left: Sketch of experimental setup (reproduced from Weiss et al. 2022). Right: detail of CMOS camera image; the full-frame image size is $2160 \times 2560\ px$.

Main IPR parameters	
Number of outer iterations	5
2D peak intensity threshold [counts]	600
Allowed triangulation error [px]	$0.6 - 0.9$
Number of shaking iterations	6
Particle tracking parameters	
Predictor (*search*/*residual*)	u_{PSC} / u_{PSC}
Search radius δ_{2p} [px]	2
Cost function terms (weight factor)	σ_I (0.5) / ε_{pred} (1.0)
σ_I^{max} [counts] / ε_{pred}^{max} [m/s]	∞ / 0.02

Table 2. Summary of TP-STB processing parameters for the Rayleigh-Bénard-convection case.

Due to the relatively low image noise and good image quality (i.e. consistent particle peak intensity for all cameras in the imaging system and over the recording sequence), a single iteration of TP-STB has been employed for the results shown in the present section; the main processing parameters are presented in Table 2.

The displacement field predictor was estimated by PSC with a final cross-correlation volume of $20 \times 20 \times 10\ px$ (approximately $2.8 \times 2.8 \times 1.4\ mm^3$).

Approximately 87% of the reference tracks ($\approx$ 290,000 tracks) are correctly reconstructed by TP-STB; the ghost particle level remains below 1% ($\approx$ 2,800 tracks).

The number of correct tracks reconstructed by TP-STB, as well as their positional error, is computed with respect to the reference tracks from TR-STB obtained after filtering the particle positions along the tracks by means of the TrackFit spline interpolation scheme (Gesemann et al 2016); the cut-off frequency of the low-pass filter is determined from the spectral distribution of the unfitted tracks in order to remove the high-frequency measurement noise and preserve the physical fluctuations.

The reference velocity values are computed by linear fit of the reference particle positions from the fitted TR-STB tracks extracted at the two time-instants used for the TP-STB processing; this allows to isolate the contribution to the velocity error associated to the random positional noise due to the IPR reconstruction. On the other hand, the truncation error due to the finite time separation between the two pulses is not included in the present analysis.

This choice is motivated, on the one hand, by the fact that the magnitude of the truncation error strongly depends on the particular investigated flow (i.e. ratio between the temporal scales and the chosen time separation between pulses). On the other hand, the smallest time separation adopted for dual-frame investigation is not a free parameter that can be changed in post-processing, but it is typically set in order to limit the maximum particle displacement between the two frames to a value that would allow a robust velocimetry analysis either by cross-correlation or particle tracking ($\approx 11\ px$ in the present investigation).

The positional and velocity analysis based on the correctly reconstructed tracks is presented in Figure 6. In the chosen reference system, the XY plane is parallel to the top and bottom plates of the cell; on the other hand, Z is aligned with the imaging system viewing direction. The finite aperture of the imaging system justifies the larger errors in the Z direction by a factor of approximately 3.5. The positional RMS errors are approximately $5\ \mu m$ ($0.04\ px$) and $19\ \mu m$ ($0.14\ px$) for X and Z respectively; the velocity RMS errors are

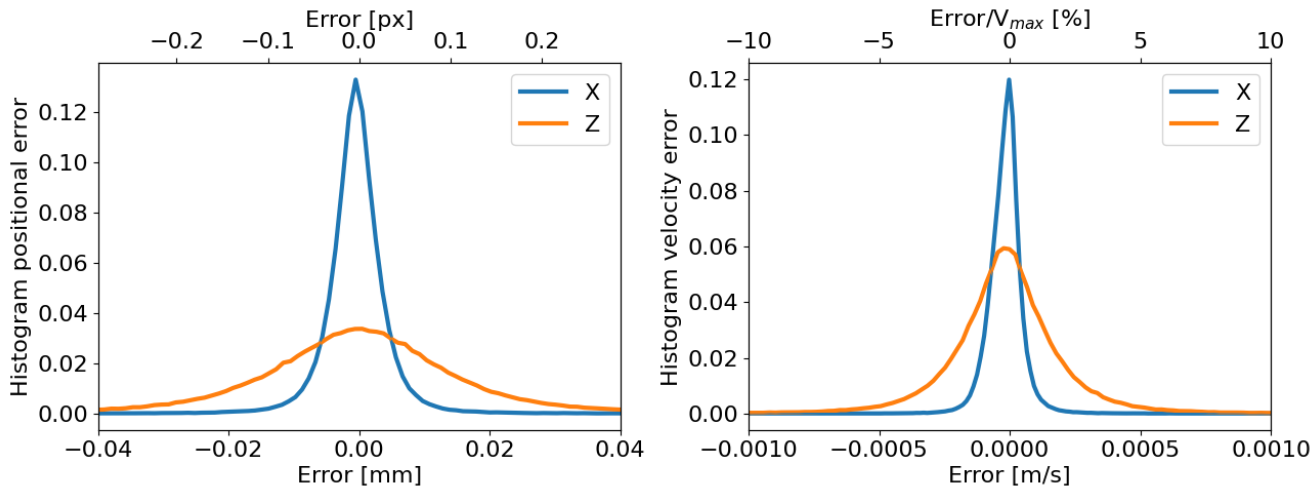

Figure 6. Histograms of the particle peak positional (left) and velocity (right) errors for the in-plane (X in blue) and out-of-plane (Z in orange) components.

approximately 0.69% V_{max} and 2.27% V_{max} for the in-plane and out-of-plane components respectively. A visualization of the 3D instantaneous tracks obtained with TP-STB is presented in Figure 7.

Acknowledgments

This work has been carried out in the context of the HOMER (Holistic Optical Metrology for Aero-Elastic Research) project, funded by the European Union's Horizon 2020 research and innovation programme under grant agreement No 769237.

The authors of Sciacchitano et al 2022 are kindly acknowledged for providing the synthetic dataset described in section 3.1. The authors of Weiss et al 2022 are kindly acknowledged for providing the experimental dataset for section 3.2.

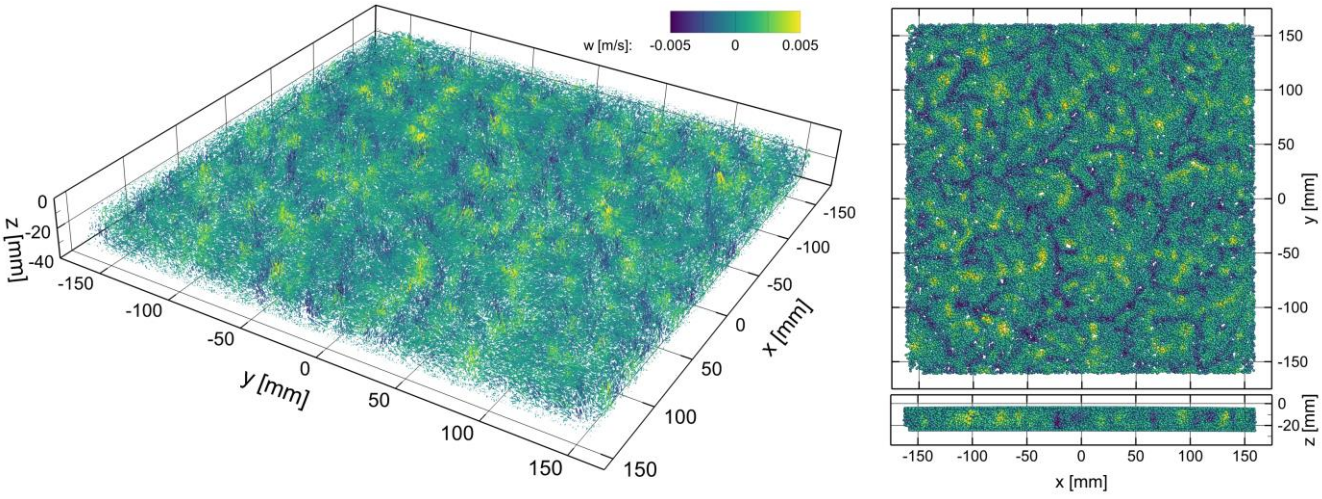

Figure 7. Instantaneous result from TP-STB; particles color-coded with the velocity component along Z. Blue indicates sinking particles while yellow indicates rising ones. Left: complete track field (approximately 290,000 particles) marked with velocity vector. Right: spherical particle markers in a 8 mm XY-slice (top) and 10 mm XZ-slice (bottom).

References

Bosbach, J., Schanz, D., Godbersen, P., & Schröder, A. (2019, September). Dense Lagrangian particle tracking of turbulent Rayleigh Bénard convection in a cylindrical sample using Shake-The-Box. In 17th European Turbulence Conference.

Cornic, P., Leclaire, B., Champagnat, F., Le Besnerais, G., Cheminet, A., Illoul, C., & Losfeld, G. (2020). Double-frame tomographic PTV at high seeding densities. Experiments in Fluids, 61(2), 1-24.

Elsinga, G. E., Scarano, F., Wieneke, B., & van Oudheusden, B. W. (2006). Tomographic particle image velocimetry. Experiments in fluids, 41(6), 933-947.

Elsinga, G. E., Westerweel, J., Scarano, F., & Novara, M. (2011). On the velocity of ghost particles and the bias errors in Tomographic-PIV. Experiments in fluids, 50(4), 825-838.

Fuchs, T., Hain, R., & Kähler, C. J. (2016). Double-frame 3D-PTV using a tomographic predictor. Experiments in Fluids, 57(11), 1-5.

Fuchs, T., Hain, R., & Kähler, C. J. (2017). Non-iterative double-frame 2D/3D particle tracking velocimetry. Experiments in Fluids, 58(9), 1-5.

Gesemann, S., Huhn, F., Schanz, D., & Schröder, A. (2016, July). From noisy particle tracks to velocity, acceleration and pressure fields using B-splines and penalties. In 18th international symposium on applications of laser and imaging techniques to fluid mechanics, Lisbon, Portugal (pp. 4-7).

Huhn, F., Schanz, D., Gesemann, S., Dierksheide, U., van de Meerendonk, R., & Schröder, A. (2017). Large-scale volumetric flow measurement in a pure thermal plume by dense tracking of helium-filled soap bubbles. Experiments in Fluids, 58(9), 1-19.

Jahn T, Schanz D, Gesemann S, Schröder A (2017) 2-Pulse STB: 3D particle tracking at high particle image densities. In: 12th international symposium on PIV–PIV17. Busan, Korea.

Jahn, T., Schanz, D. & Schröder, A. (2021). Advanced iterative particle reconstruction for Lagrangian particle tracking. Exp Fluids 62, 179.

Kähler, C. J., Astarita, T., Vlachos, P. P., Sakakibara, J., Hain, R., Discetti, S., ... & Cierpka, C. (2016). Main results of the 4th International PIV Challenge. Experiments in Fluids, 57(6), 97.

Lasinger, K., Vogel, C., Pock, T., & Schindler, K. (2020). 3D fluid flow estimation with integrated particle reconstruction. International Journal of Computer Vision, 128(4), 1012-1027.

Leclaire, B., Mary, I., Liauzun, C., Péron, S., Sciacchitano, A., Schröder, A., ... & Champagnat, F. (2021, August). First challenge on Lagrangian Particle Tracking and Data Assimilation: datasets description and planned evolution to an open online benchmark. In 14th International Symposium on Particle Image Velocimetry (Vol. 1, No. 1).

Lynch, K. P., & Scarano, F. (2015). An efficient and accurate approach to MTE-MART for time-resolved tomographic PIV. Experiments in Fluids, 56(3), 1-16.

Novara, M., Batenburg, K. J., & Scarano, F. (2010). Motion tracking-enhanced MART for tomographic PIV. Measurement science and technology, 21(3), 035401.

Novara, M., Schanz, D., Geisler, R., Gesemann, S., Voss, C., & Schröder, A. (2019). Multi-exposed recordings for 3D Lagrangian particle tracking with Multi-Pulse Shake-The-Box. Experiments in Fluids, 60(3), 44.

Novara, M., Schanz, D., Gesemann, S., Lynch, K., & Schröder, A. (2016b). Lagrangian 3D particle tracking for multi-pulse systems: performance assessment and application of Shake-The-Box. In 18th international symposium on applications of laser and imaging techniques to fluid mechanics, Lisbon, Portugal.

Novara, M., Schanz, D., Reuther, N., Kähler, C. J., & Schröder, A. (2016a). Lagrangian 3D particle tracking in high-speed flows: Shake-The-Box for multi-pulse systems. Experiments in Fluids, 57(8), 128.

Scarano, F. (2012). Tomographic PIV: principles and practice. Measurement Science and Technology, 24(1), 012001.

Scarano, F., & Poelma, C. (2009). Three-dimensional vorticity patterns of cylinder wakes. Experiments in Fluids, 47(1), 69-83.

Schanz, D., Gesemann, S., & Schröder, A. (2016). Shake-The-Box: Lagrangian particle tracking at high particle image densities. Experiments in fluids, 57(5), 70.

Schneiders, J. F., & Scarano, F. (2016). Dense velocity reconstruction from tomographic PTV with material derivatives. Experiments in fluids, 57(9), 1-22.

Sciacchitano, A., Leclaire, B., & Schroeder, A. (2021, August). Main results of the first lagrangian particle tracking challenge. In 14th International Symposium on Particle Image Velocimetry (Vol. 1, No. 1).

Sciacchitano, A., Leclaire, B., & Schroeder, A. (2022). Main results of the analysis of the HOMER Lagrangian Particle Tracking and Data Assimilation database. In 20th international symposium on applications of laser and imaging techniques to fluid mechanics, Lisbon, Portugal.

Weiss S, Schanz D, Erdogdu AO, Schröder A, Bosbach J (2022) Investigation of turbulent superstructures in Rayleigh-Bénard convection by Lagrangian particle tracking of fluorescent microspheres. In 20th international symposium on applications of laser and imaging techniques to fluid mechanics, Lisbon, Portugal.

Wieneke, B. (2013). Iterative reconstruction of volumetric particle distribution. Measurement Science and Technology, 24(2), 024008.